Supporting Upper Limb Movements with a Soft Robot after a Brachial Plexus Injury

- Supplementary Materials -

Roberto Ferroni*[1], Vittoria Aglietta*[2], Daniele Filippo Mauceri[1], Jacopo Carpaneto[1], Silvestro Micera[1,3,4], Paolo Titolo*[5], Tommaso Proietti*†[1,4]

* These authors contributed equally.
† Corresponding author: tommaso.proietti@santannapisa.it

[1] The Biorobotics Institute and Department of Excellence in Robotics & AI, Scuola Superiore Sant'Anna, Pisa, Italy
[2] Division of Physical Medicine and Rehabilitation, Department of Surgical Sciences, University of Turin, Turin, Italy
[3] Translational NeuroEngineering Laboratory, Neuro-X Institute, School of Engineering, École Polytechnique Fédérale de Lausanne (EPFL), Lausanne, Switzerland
[4] Modular Implantable Neuroprostheses (MINE) Laboratory, Università Vita-Salute San Raffaele, Milano, Italy
[5] OU Traumatology-Reconstructive Microsurgery, Department of Orthopaedics and Traumatology, CTO Hospital, Turin, Italy

Supplementary Methods: Control architecture and pneumatic control unit

The exosuit was controlled through a two-layer architecture composed of a high-level kinematics-based assistance policy and a low-level pneumatic pressure controller, as show in Fig. S1. Upper-limb motion was measured by inertial measurement units (IMUs, *Bosch BNO055*) mounted on the upper arm and forearm, and joint kinematics were reconstructed in real time from the IMU quaternions. In particular, the reconstructed kinematics referred to shoulder elevation (either abduction or flexion), shoulder horizontal flexion, elbow flexion/extension, and trunk 3D rotations. The resulting arm kinematics were used to estimate user intention and to trigger or modulate assistance in a subject-specific manner, similarly to our previous work *(1)*. In the present study, the control approach relied on residual volitional motion; therefore, assistance could only be triggered when the participant generated a detectable kinematic command. This design was intentional, as it kept the user actively engaged in the movement and reduced the risk of passive driving of the limb.

At the high level, shoulder assistance was implemented as a gravity-compensation strategy based on a subject-specific look-up table that mapped arm orientation to a desired pressure command *(2)*. This mapping was calibrated for each participant before testing to maximize comfortable support while preserving voluntary movement, see Fig. S2.C. Specifically, participants were asked to remain passive while the robot was slowly inflated, generating pressure-versus-angle maps during both inflation and venting to account for hysteresis. These maps were then used as a look-up table to infer the pressure required to provide approximately 100% assistance at a given angle.

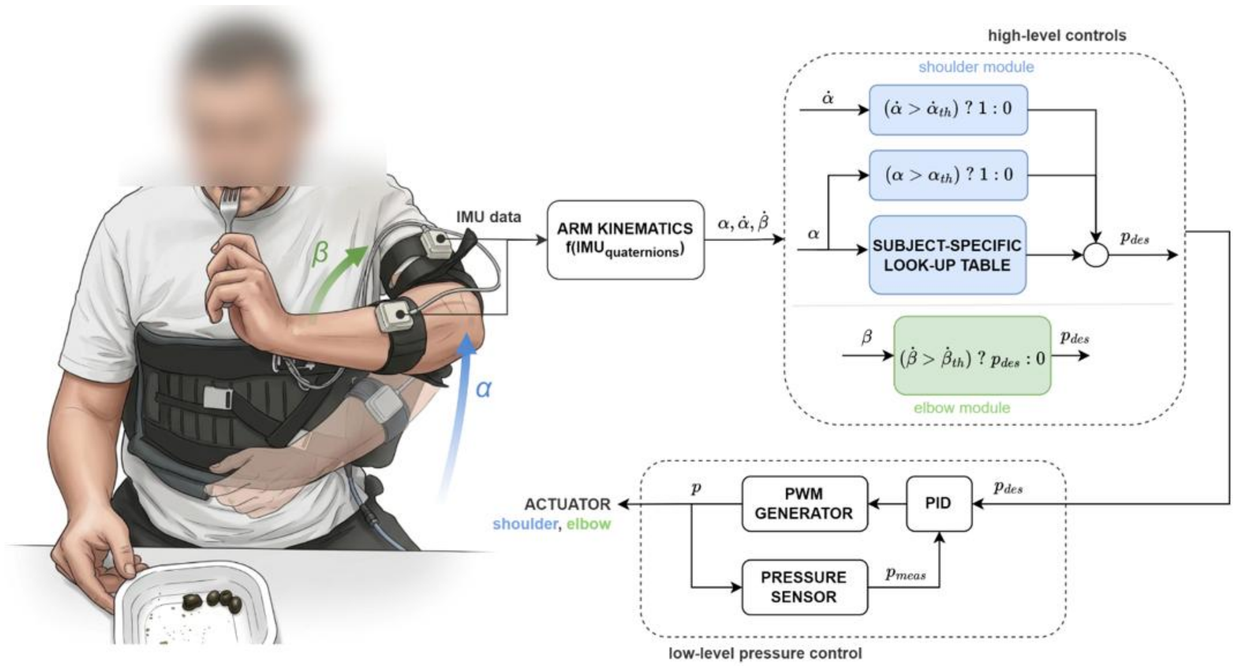

Supplementary Figure S1: Control architecture of the soft exosuit. The system uses three inertial measurement units (IMUs) to estimate upper-limb kinematics from torso, upper-arm, and forearm orientation. At the high-level control layer, shoulder assistance is generated through a subject-specific look-up table that maps arm kinematics to the desired shoulder pressure p_{des}. The assistance is active or not depending on two intention-detection tests, based on both direction (α) and velocity of movement ($\dot{\alpha}$). The look-up table is built via a simple calibration requiring inflation of the actuator while the participant is passive. Elbow assistance, instead, is triggered when the estimated elbow motion exceeds a subject-specific angular velocity threshold $\dot{\beta}_{th}$. The low-level pressure controller regulates actuator pressure using closed-loop feedback from the pressure sensor and a proportiona-integral-derivative (PID) controller, which drives the PWM generator and pneumatic actuator.

Importantly, the assistance was activated only upon reaching a minimum volitional elevation threshold and following the detection of upward movement via angular velocity. Both parameters were tailored to each participant during the initial calibration phase, see Fig. S2.A. Elbow assistance, instead, used a triggered passive strategy: movement initiation was detected from the IMU-derived elbow angular velocity, and when the estimated velocity exceeded a subject-specific threshold, the elbow actuator was inflated to a predetermined pressure value (Fig. S2.B). The set pressure value was adjusted during the calibration phase to accommodate participant comfort. Moreover, for both controllers, calibration was also used to account for residual control and movement strategy, including compensation patterns when present. The actuators were manually vented via the graphical user interface once each movement/repetition was completed. While this approach was appropriate for the controlled testing environment used in the present study, it is not well suited to real-life ADL support, where continuously varying elbow and shoulder angles are required. The shoulder controller can already manage both inflation and venting because of its continuous control strategy; in contrast, the current elbow triggered-passive mode will require further development to enable more continuous operation in less structured settings.

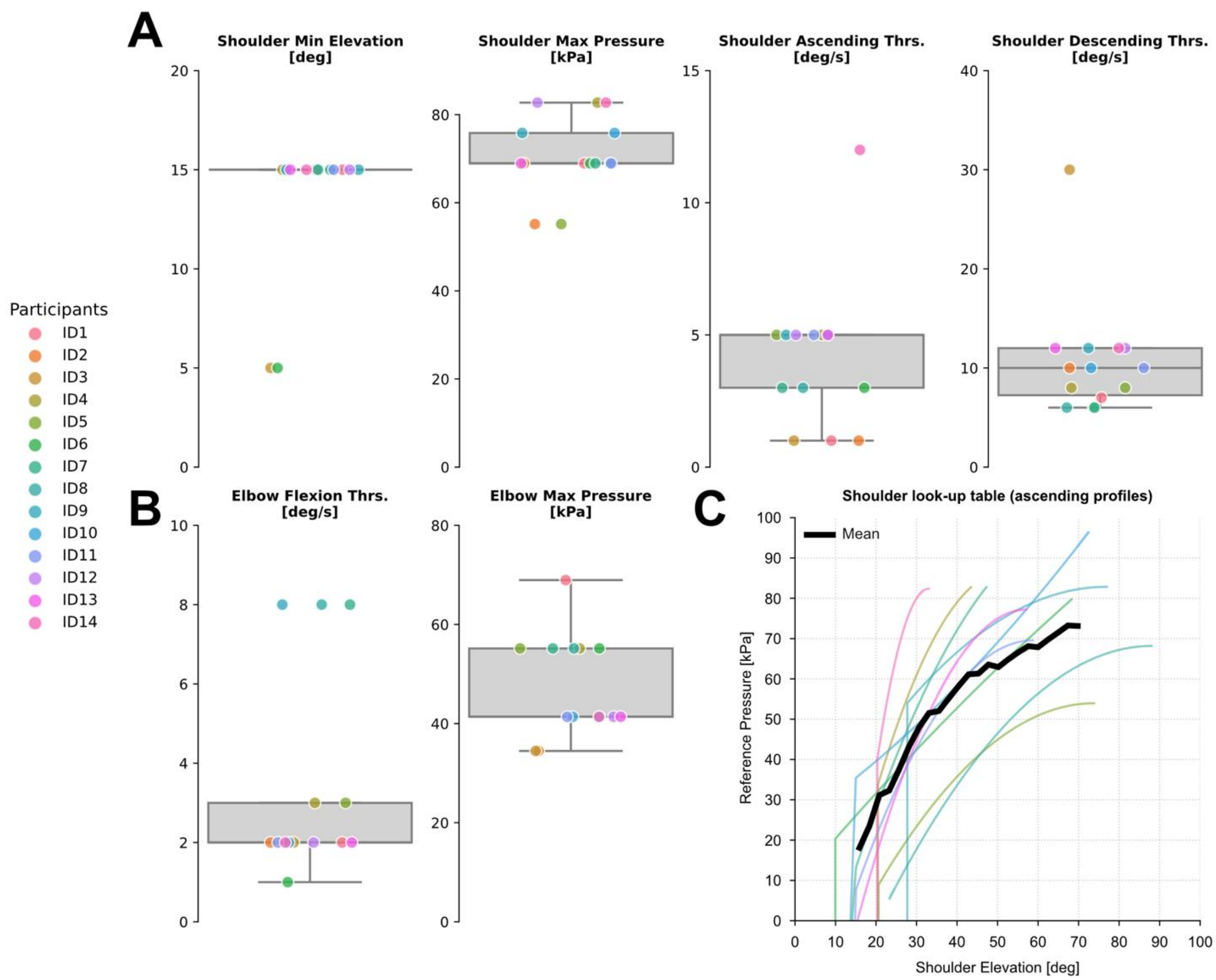

Supplementary Figure S2: Calibration parameters across participants. In all panels, colored markers/lines identify individual participants (see legend). (A) Shoulder-related configuration parameters: distribution of minimum shoulder elevation (below this value, the assistance did not start), maximum calibration pressure (safety saturation), and angular velocity thresholds for ascending and descending movement detection. Boxplots show the median (centre line), interquartile range (box), and whiskers extending to 1.5× the interquartile range; dots indicate individual observations. (B) Elbow-related configuration parameters: distribution of flexion angular velocity thresholds ($\dot{\beta_{th}}$) and maximum flexion pressures (corresponding to p_{des}). (C) Shoulder look-up table profiles (inflation). The solid black line indicates the population average within the monotonic functional range (15°–70°).

At the low level, actuator pressure was regulated by a custom benchtop pneumatic control unit. The control box integrated two miniature air pumps (*Schwarzer Precision GmbH*, Germany), normally closed solenoid valves for inflation, venting and exhaust (*Emerson Electric Co.*, USA), a microcontroller (Feather M0 Wifi, *Adafruit*, USA), and pressure sensors placed in the actuator line (ABP Series, *Honeywell International Inc.*, USA). The microcontroller executed a pressure regulation loop at 100 Hz using a PID-based control stage driving the PWM generator. This architecture enabled pressure tracking during both inflation and deflation and allowed the actuators to operate independently while sharing the same hardware platform. The pneumatic control box was wall-powered and weighed 2.1 kg (22 cm × 14 cm × 30 cm); the system was connected to the wearable modules through pneumatic tubing routed to minimize interference with upper-limb motion. The IMUs streamed data with the control unit via TCP/IP (WiFi), using a battery-powered microcontroller (Feather M0 Wifi, *Adafruit*, USA). The control unit produces 52.0 dB of ambient noise, peaking at 57.5 dB when the pumps are active. Noise measurements were taken with a sound level meter (72-942, Multicomp Pro, USA) in a 42 dB noise environment, placing the system's acoustic emissions within the range of a normal conversation *(3)*.

The temporal performance of the system, including actuator rise time (t_{90}) and the delay between movement onset and controller activation, is quantitatively characterized in Fig. S3.

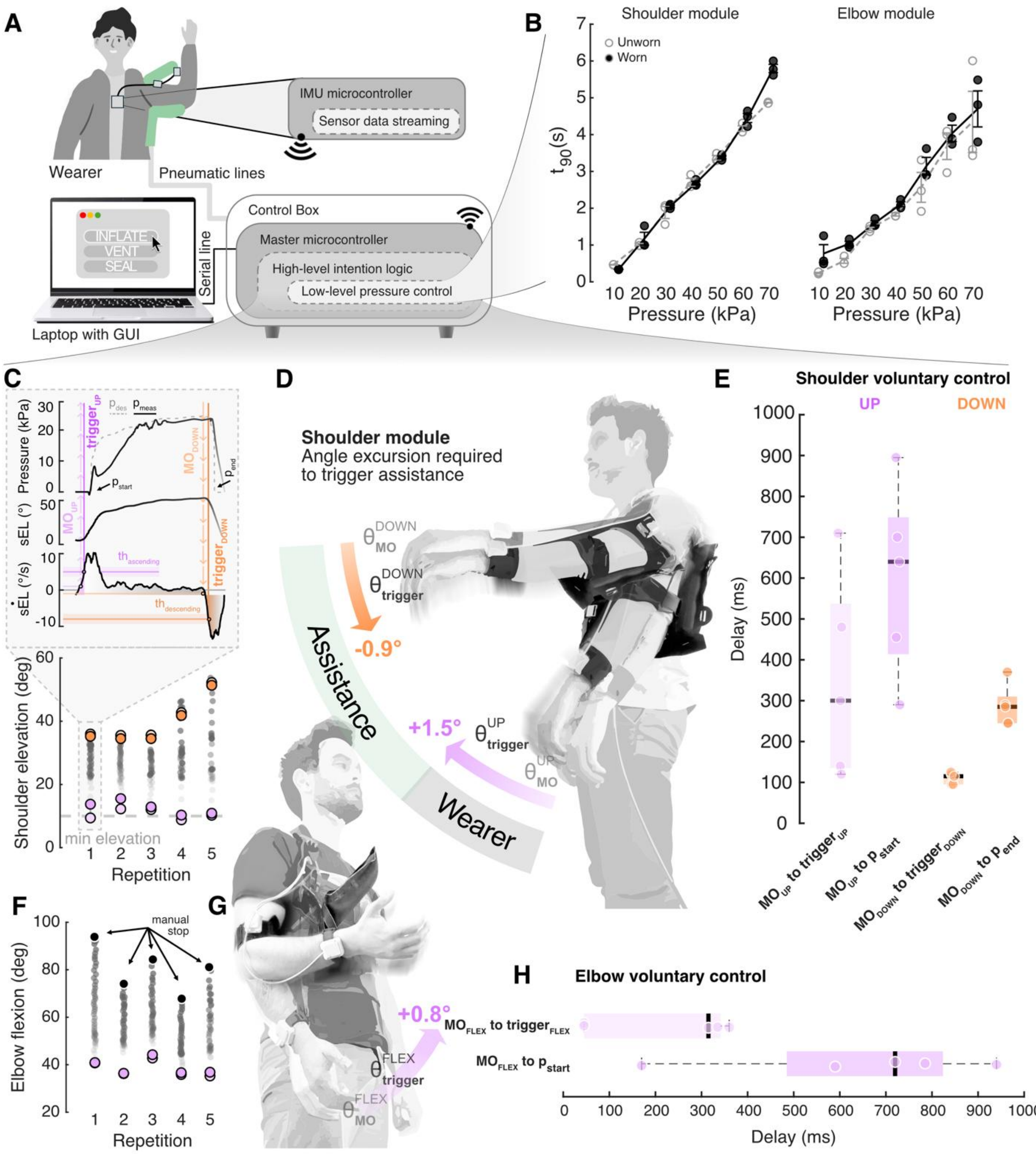

Supplementary Figure S3: System architecture and temporal performance of the control strategy. (A) System overview and control architecture. The wearable exosuit integrates IMU sensors connected to a dedicated microcontroller that streams kinematic data via TCP/IP to the control box. The control box, interfaced with a laptop GUI, executes both the high-level intention detection logic and the low-level pressure regulation, driving the pneumatic actuation modules. (B) Rise time (t_{90}) of the shoulder and elbow modules, defined as the time required to reach 90% of the target pressure, measured across pressure levels (10-70 kPa, 10 kPa increments). For each condition, N = 3 repetitions are shown along with mean ± standard deviation. Tests were performed both in unworn condition, and with the actuator worn by a representative subject (male, 174 cm, 70 kg). (C – E) High-level voluntary control for the shoulder module. (C) Top: representative time-series of actuator pressure, shoulder elevation (sEL), and shoulder angular velocity ($\dot{sEL}$), illustrating a typical control cycle from rest to upward movement onset (MO_{UP}), trigger of assistance upon exceeding the ascending velocity threshold ($trigger_{UP}$), pressure setpoint assignment via the subject-specific look-up table, and subsequent downward movement onset (MO_{DOWN}), $trigger_{DOWN}$, and assistance termination. Bottom: scatter plot of shoulder elevation trajectories across N = 5 repetitions, highlighting initial and final angles during voluntary up-down movements. (D) Illustration of the median angular excursion required by the user to trigger assistance during upward and downward movements, computed as the difference between movement onset and controller trigger. (E) Temporal delays: (1) from MO to threshold crossing (trigger), and (2) from MO to pressure onset (p_{start}), defined as the first instant at which actuator pressure exceeds 0 kPa. Analogous metrics are reported for both upward and downward phases. N = 5 repetitions. (F – H) High-level voluntary control for the elbow module. (F) Scatter plot of elbow flexion trajectories across N = 5 repetitions, from flexion onset (MO_{FLEX}) to trigger ($trigger_{FLEX}$) and subsequent attainment of the personalized pressure setpoint. Movement termination was manually defined via the GUI. (G) Illustration of the angular excursion required to trigger elbow flexion assistance. (H) Temporal delays between MO_{FLEX} and (1) $trigger_{FLEX}$ (threshold crossing), and (2) p_{start} (onset of actuator pressurization). Thresholds and pressure setpoints used in these experiments correspond to the median values observed across N = 8 participants in the BPI study. Movement speed was natural and not strictly controlled, to reflect realistic operating conditions consistent with the experimental protocol. Boxplots (E-H) show the median (centre line), interquartile range (box), and whiskers extending to 1.5× the interquartile range; dots indicate individual paired observations.

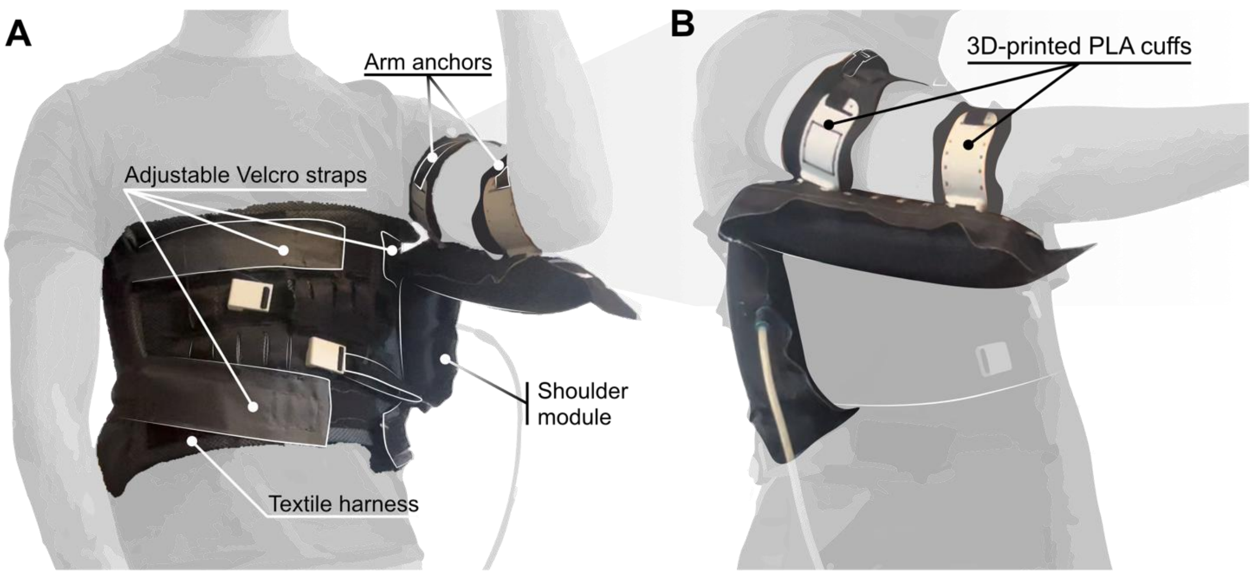

Supplementary Figure S4: Human-robot interface of the shoulder module. (A) Overview of the interface design, showing the shoulder module connected to a custom textile harness worn on the trunk, featuring adjustable Velcro straps for fit and load distribution. The module is anchored to the upper arm through dedicated arm anchors. (B) Detailed view of the 3D-printed arm cuffs used as rigid anchors to interface with the upper arm. The cuffs incorporate an integrated neoprene lining, ensuring safe and comfortable contact with the skin. While effective in enabling load transfer, these cuffs represent a critical rigid interconnection within an otherwise compliant system and were occasionally prone to mechanical failure during testing. This highlights the need for further design refinement of this component in future iterations.

ID	Shoulder Flexion	Shoulder Abduction	Elbow Flexion
ID1	123.3	119.4	13.8
ID2	14.7	20.3	70.3
ID3	23.7	23.6	41.1
ID4	41.8	26.4	137.1 *
ID5	11.5	10.8	15.1
ID6	19.2	20.9	133.5 *
ID7	88.0	64.0	145.4 *
ID8	35.9	31.2	80.7
ID9	33.5	27.0	5.4
ID10	51.7	43.4	142.9 *
ID11	33.4	27.1	42.4
ID12	49.4	39.1	128.9 *
ID13	30.1	21.7	139.4 *
ID14	16.4	16.5	10.7
MEDIAN			
(N = 14)	**33.5**	**26.7**	**75.5**
(N = 8)	**-**	**-**	**28.1**

Supplementary Table S1: Participant baseline range of motion (ROM). Angular values are reported in degrees for all 14 participants. Participants with near-physiological elbow flexion ROM (>90°; N = 6, marked with *) were not tested with the elbow module and therefore only received shoulder assistance during the experimental protocol.

ID	ROM Task Shoulder Flexion	Shoulder Abduction	Elbow Flexion	Endurance Task Duration	AD	MD	PD	PECT	BIC	TRIC	BORG	ARAT
ID1	6.8	-2.0	643.6	26.6	-28.7	-31.1	0.5	-27.2	-59.1	-97.6	-6	-
ID2	168.0	114.8	148.4	0.0	8.5	4.2	3.6	1.9	-18.1	-17.2	-1	-
ID3	132.9	121.3	133.4	121.5	-50.0	-79.8	-84.9	-60.0	-91.5	-79.0	-8	-
ID4	95.5	141.8	-	84.9	-55.8	-30.1	-19.7	-	-52.2	-47.0	-6	2
ID5	155.7	146.9	203.8	39.3	-47.6	-50.2	-56.5	-69.0	-77.4	-54.8	-3	-
ID6	45.9	118.6	-	137.8	-40.5	-26.8	-21.8	-47.4	-7.8	-	0	7
ID7	16.2	40.5	-	87.6	-46.3	-33.5	-43.5	-64.9	-32.3	-52.5	-5	3
ID8	90.6	100.9	13.0	13.7	-71.2	-79.7	-45.4	-74.8	-91.5	-	-7	-
ID9	89.9	104.8	366.3	150.9	40.6	-79.3	-75.8	-79.1	-76.2	-72.9	-2.5	-
ID10	76.6	42.7	-	0.0	-50.5	-67.4	-65.0	-42.6	-64.3	-73.1	-1	-
ID11	108.4	140.5	162.3	135.6	-8.3	22.0	3.9	-77.3	-55.7	121.2	-6	-
ID12	41.0	117.3	-	124.9	-31.6	-48.8	-24.9	-	-19.8	-33.0	-5	6
ID13	13.5	32.2	-	114.4	-	-	-	-	-	-	-2	-
ID14	300.8	297.8	768.9	180.0	-	-	-	-	-	-	-	-
MEDIAN	**90.3**	**116.1**	**183.1**	**101.0**	**-43.4**	**-41.2**	**-34.2**	**-62.5**	**-57.4**	**-53.6**	**-5**	**-**

Supplementary Table S2: Participant-level key outcomes. Shown are robot-off/robot-on changes for shoulder/elbow ROM (% change), endurance task duration (Δ seconds) and associated EMG activity (% change vs MVC, AD = anterior deltoid, MD = middle deltoid, PD = posterior deltoid, PECT = pectoralis major, BIC = biceps, TRIC = triceps), and Borg perceived exertion (absolute change), and ARAT scores (absolute change). Elbow outcomes (N=8) reflect participants with baseline elbow ROM <90°; ARAT/ADL tasks (N=4) reflect participants with sufficient hand function.

Supplementary References

1. R. Ferroni, A multi-joint soft exosuit improves shoulder and elbow motor functions in individuals with spinal cord injury. *Nat. Mach. Intell.* (2025).

2. T. Proietti, C. O'Neill, C. J. Hohimer, K. Nuckols, M. E. Clarke, Y. M. Zhou, D. J. Lin, C. J. Walsh, Sensing and Control of a Multi-Joint Soft Wearable Robot for Upper-Limb Assistance and Rehabilitation. *IEEE Robot. Autom. Lett.* **6**, 2381–2388 (2021).

3. Berglund, Birgitta, Lindvall, Thomas, Schwela, Dietrich H & World Health Organization. Occupational and Environmental Health Team (1999). Guidelines for community noise. World Health Organization. https://iris.who.int/handle/10665/66217